Design and Modeling of Micro-glassblown Inverted-wineglass Structures

Doruk Senkal, Mohammed J. Ahamed, and Andrei M. Shkel
MicroSystems Laboratory, University of California, Irvine, CA, USA
Email: {dsenkal, mahamed, ashkel}@uci.edu

***Abstract*— This paper reports analytical and finite element models for predicting the final 3-D geometry of micro-glassblown inverted-wineglass and hemi-toroidal structures from a set of initial conditions. Using these methods critical geometric parameters for wineglass resonator and gyroscope operation, such as shell thickness, shell height, stem type (hollow/solid), and stem diameter can be estimated from initial parameters. Analytical models for first order calculation of shell height and minor radius, as well as finite element models based on Arbitrary Lagrangian-Eulerian (ALE) methods for calculating the thickness of the shell and diameter of the stem structure are presented. Developed models were validated against fabricated micro-glassblown structures and showed better than 10 % match to experimental results. Methods presented in this paper can be used to design micro-glassblown wineglass resonators with specific dimensions and resonance frequencies, essentially taking the guesswork out of the design process and significantly lowering the development time.**

I. Introduction

Recently, there has been a growing interest in 3-D MEMS wineglass resonator architectures for use in timing and inertial sensing applications due to potential advantages in symmetry, minimization of energy losses, and immunity to external vibrations [1].

Two common themes emerged in the literature for wafer-level fabrication of micro-wineglass structures: (1) thin-film deposition of the resonator material into a pre-defined mold [2]–[4] and (2) pressure induced plastic deformation of a device layer to form the 3-D shell structure (micro-glassblowing) [5]. Due to the self-correcting behavior of surface tension forces, micro-glassblowing process has potential advantages over conventional micro-machining techniques in terms of surface roughness, structural symmetry, and robustness to fabrication imperfections. For this reason similar fabrication processes emerged in the recent years, which rely on plastic deformation of the device layer to create micro-wineglass structures for rate integrating gyroscope and resonator applications. These processes include blow molding of bulk metallic glasses [6], micro-glassblowing of fused silica/ULE inverted-wineglass structures [7], [8], Fig. 1, and blow-torch molding of fused silica hemi-toroidal structures [9].

This material is based upon work supported by DARPA grant W31P4Q-11-1-0006 (Program Manager Dr. Robert Lutwak).

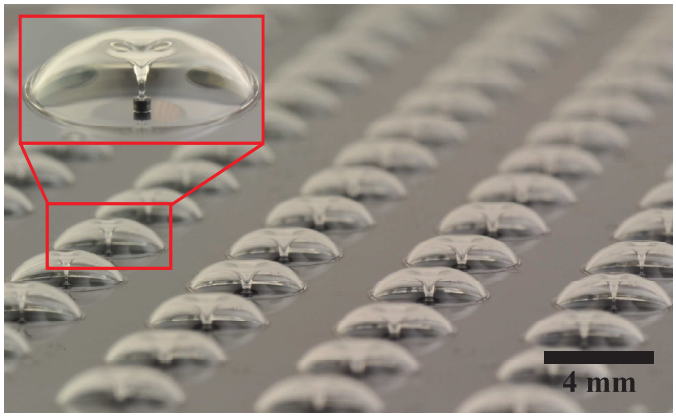

Fig. 1. Micro-glassblowing process can create arrays of inverted-wineglass structures on the wafer surface. Outer diameter of shells is 4 mm, over 100 shells were fabricated on a 4" wafer.

Despite the recent advances in fabrication techniques for micro-glassblown structures, means to design a specific 3-D geometry based on initial geometric parameters have so far not been presented. Even though, a set of equations to predict the final geometry of micro-glassblown spherical shell structures were introduced in [10], accurate estimation of shell thickness was not possible and the equations did not extend to inverted-wineglass structures. This paper presents analytical and finite element models to predict the outcome of the micro-glassblowing process, which enables one to design photomasks and process parameters to obtain a specific 3-D shell geometry.

II. Design & Modeling

In this section, first a brief description of the micro-glassblowing process will be presented. This will be followed by analytical expressions to predict the final micro-glassblown geometry and finite element methods to predict thickness of the shell structure and stem diameter.

A. Micro-glassblowing of Inverted-wineglass Structures

Micro-glassblowing process consists of four fundamental steps: (1) etching of cavities onto a substrate wafer, (2) bonding of a thin glass layer on top as to trap atmospheric

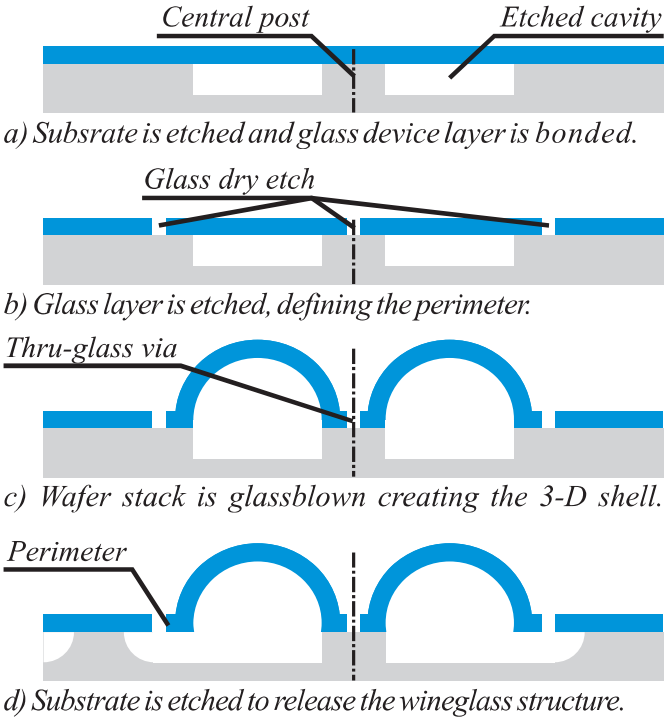

Fig. 2. Fabrication of inverted wineglass structures consists of cavity etch, bonding, micro-glassblowing, and perimeter release.

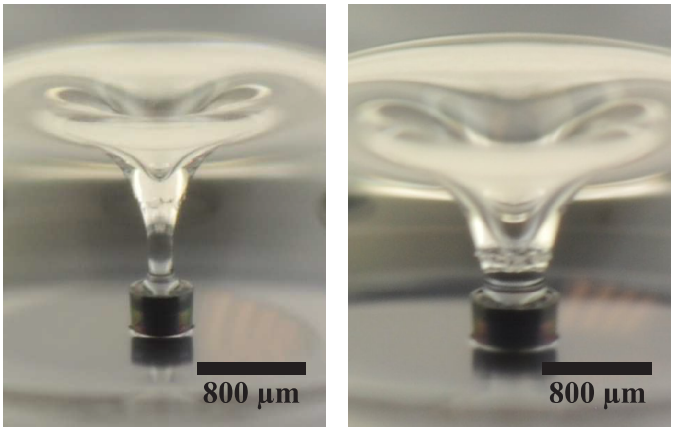

Fig. 3. Small central post diameters create solid stem structures (left), large diameters create hemi-toroidal structures (right).

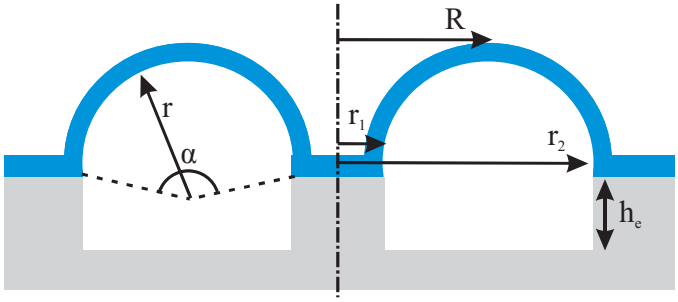

Fig. 4. Geometric parameters of an inverted-wineglass structure: Minor radius r, major radius R, inner perimeter r_1, outer perimeter r_2 and etch depth h_e.

pressure air inside the cavities, Fig. 2(a), and (3) glassblowing at an elevated temperature which softens the glass layer and causes the air inside the cavities to expand, forming the 3-D shell structure, Fig. 2(c). To create wineglass structures the process typically involves an additional step (4) etching or lapping for perimeter release, Fig. 2(d) and a metallization step for electrical conductivity. At the end of the fabrication process, arrays of shell structures are created on the surface of the wafer, Fig. 3. Final device geometry heavily depends on the photolithographic pattern on the wafer surface as well as the etch depth of the cavity. For example, solid self-aligned stem structures were obtained for a central post diameter of 400 μm, whereas hollow hemi-toroidal structures were obtained for a central post diameter of 600 μm, Fig. 1. For this reason an accurate method to estimate the final geometry from initial dimensions is required.

B. Analytical Solution

In this section analytical expressions for predicting the dimensions of the final inverted-wineglass structure are derived. These expressions can be used to calculate height and minor radius of the structure (h and r) based on the initial cavity dimensions. These expressions assume ideal hemi-toroidal shell structures with zero thickness, as such it is not possible to predict the thickness of the wineglass shell or the diameter of the stem structure.

Calculation starts by finding the volume of the etched cavity.

$$V_{cavity} = \pi(r_2^2 - r_1^2)h_e \,, \tag{1}$$

where r_2 is the outer perimeter of the cavity, r_1 is the perimeter of the central post and h_e is the etch depth, Fig. 4. Upon heating, air inside the cavity will expand to fill the volume of the wineglass shell according to:

$$V_{wineglass} = (\frac{T_{final}}{T_{initial}} - 1)V_{cavity} \,, \tag{2}$$

where $T_{initial}$ and T_{final} are initial and final glass-blowing temperatures in degree Kelvin. It is assumed that the air inside the cavity is at atmospheric pressure, which is also the pressure of the glassblowing chamber. The volume of the wineglass can also be calculated from geometric parameters using:

$$V_{wineglass} = \pi R r^2(\alpha - \sin(\alpha)) \tag{3}$$

where r is the minor radius, R is the major radius of the partial toroid and α is the fullness parameter in radians, Fig. 4. Minor and major radii can be removed from the above expression using:

$$r = \frac{r_2 - r_1}{2\sin(\alpha/2)}, \; R = \frac{r_1 + r_2}{2} \,. \tag{4}$$

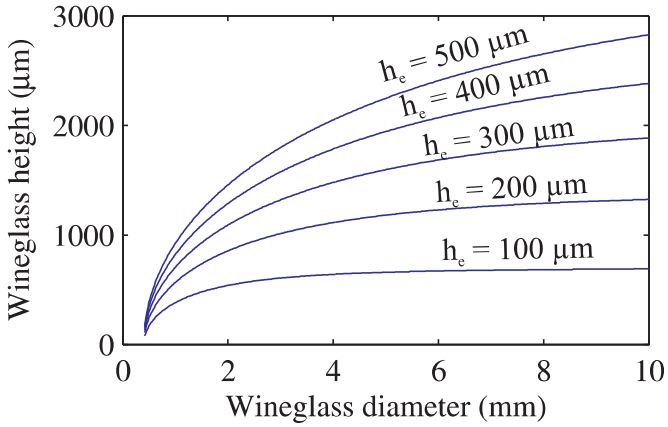

Fig. 5. Analytical solution of etch depth vs final inverted wineglass height (h_e: etch depth, stem OD is 400 μm). Glassblowing temperature is 875 °C.

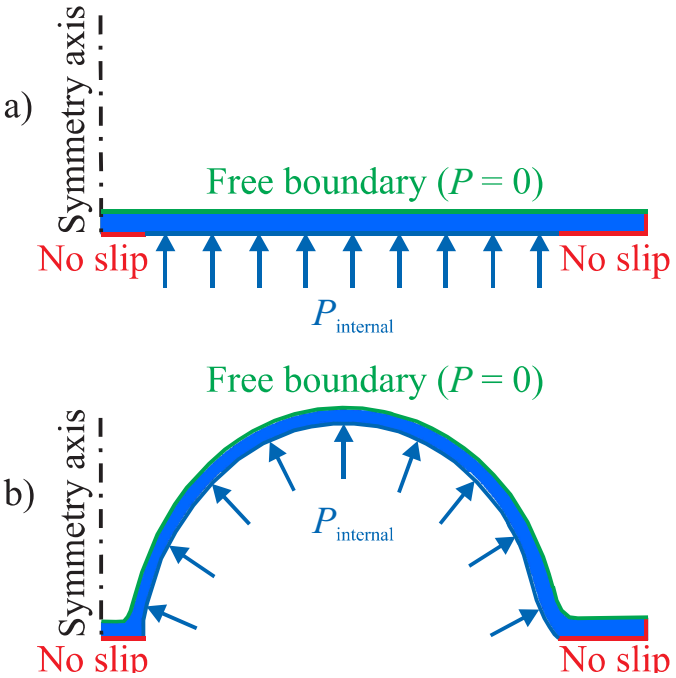

Fig. 6. Boundary conditions for finite element analysis: (a) before glassblowing, (b) after glassblowing.

Substituting (1) into (2) and (4) into (3) leaves α to be the only unknown variable, which can be solved numerically. Once α is known, all other parameters of the glassblown shell structure can be extracted using geometric relationships in Fig. 4. Solutions of these expressions for a large variety of micro-wineglass structures are presented in Fig. 5. The expressions presented in this section are not sufficient to calculate the shell thickness or the stem diameter, finite element methods to calculate these parameters will be presented in the next section.

C. Finite Element Analysis

As mentioned in the previous section, analytical expressions presented in (1) through (4) are not sufficient to predict the shell thickness and the stem diameter. For this reason finite element method (FEM) models for micro-glassblowing process were developed to predict the effect of subtle changes in initial dimensions on the final geometry.

Due to the large deformation of the shell structure, Arbitrary Lagrangian-Eulerian (ALE) technique [11], [12] was used. ALE allows the mesh to deform as to track the deformation of the structure in the time domain and reapply the boundary conditions at every time step. Comsol Multiphysics Package was used for the analysis, the following assumptions were used for boundary conditions:

- At the glassblowing temperature ($>$ 850 °C for borosilicate glass and $>$ 1600 °C for fused silica, the deformation of the glass can be modeled using viscous fluid flow with a viscosity of $10^3 - 10^6$ Pa $\cdot$ s [13].
- The driving force is a slowly varying (quasi-static) uniform pressure field within the shell cavity, Fig. 6.
- Outer surface of the shell is exposed to atmospheric pressure ($P_{gage} = 0$).
- The surfaces that are bonded to the substrate are not moving (no-slip condition).
- The shells are axi-symmetric as such a 2-D axi-symmetric model with $<$ 1000 elements is sufficient for solution.

Using the above assumptions, the gage pressure inside the cavity can be written as:

$$P_{internal} = \frac{T_{final} P_{initial} V_{cavity}}{T_{initial}(V_{cavity} + V_{wineglass})} - P_{initial}\,, \quad (5)$$

where T is the temperature in ° Kelvin and $P_{internal}$ is applied uniformly to the inner surface of the micro-wineglass structure during glassblowing, Fig. 6.

Since the volume of the wineglass will continuously change during the transient solution, (3) can not be used to calculate $V_{wineglass}$. Instead, a surface integral for the inner surface of the wineglass is used:

$$V_{wineglass} = \oint 2\pi r'^2 dnr\,, \quad (6)$$

where r' is the distance of any point in the shell structure from the symmetry axis and dnr is the projection of the infinitesimal surface area onto the symmetry axis. (6) allows continuous calculation of the shell volume and consequently the cavity pressure as the structure deforms. This allows the model to reach equilibrium when the final volume is reached ($P_{internal} = 0$).

Fig. 7 shows time domain solution of the micro-glassblowing process and the formation of the self-aligned stem structure. Decreasing the central post diameter from

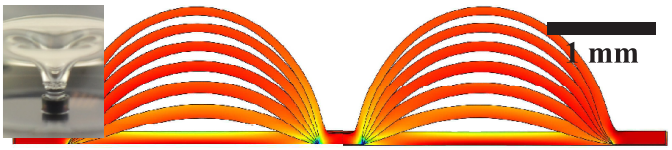

a) 400 μm stem OD creates a hemi-toroidal structure.

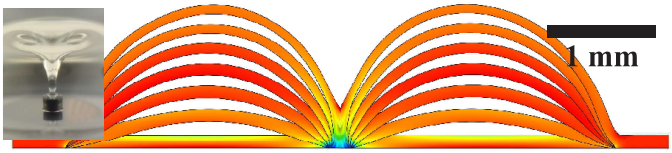

b) 200 μm stem OD creates a mushroom structure.

Fig. 7. Transient FEA of micro-glassblowing process showing the formation of self-aligned stem structures.

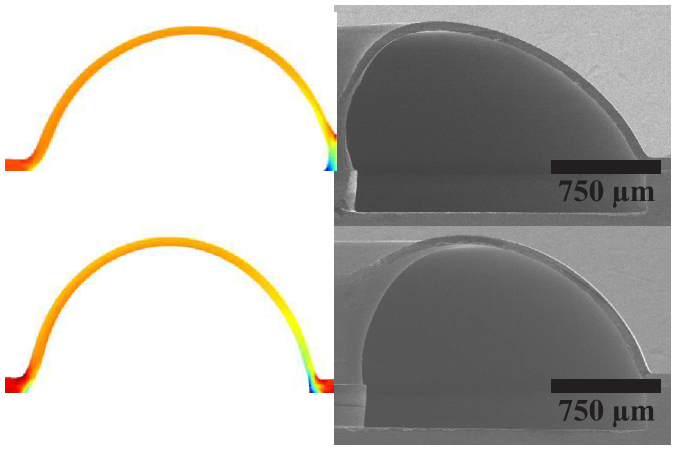

Fig. 8. Finite elemet predictions and cross-sectional SEM shots of fabricated micro-wineglass structures.

400 μm to 200 μm is sufficient to change the shell structure from a hemi-toroidal geometry to an inverted-wineglass with a solid stem structure. Fig. 8 shows a side-by-side comparison of the finite element models and the actual fabricated geometries. The results from the models are compared to cross-sectional SEM shots in Table I, showing better than 10 % accuracy.

III. Conclusion

Analytical and finite element solutions of micro-glassblown inverted-wineglass structures have been presented in this paper. Using these methods critical geometric parameters for wineglass resonator and gyroscope operation, such as shell thickness, shell height, stem type (hollow/solid) and stem diameter can be estimated from initial parameters. Developed models were validated against fabricated micro-glassblown structures and showed better than 10 % match to experimental results. Models developed in this paper can be used to design micro-glassblown structures with different geometries and sizes, enabling accurate design of micro-glassblown resonators as well as other micro-glassblown MEMS devices such as optical and micro-fluidic systems.

TABLE I

Comparison of wineglass dimensions obtained from analytical solutions, FEA and experiments.

		Device # 1	Device # 2
Initial thickness (μm)		80	300
Outer diameter (mm)		4.2	4.2
Etch depth (μm)		240	200
Glassblowing temperature (°C)		875	1700
Analytical	Final Height (μm)	971	1182
	Thickness (μm)	N/A	N/A
FEA	Final Height (μm)	1025	1260
	Thickness (μm)	52	205
Experimental	Final Height (μm)	832	1288
	Thickness (μm)	44	229

References

[1] D M Rozelle. The hemispherical resonator gyro: From wineglass to the planets. In *Proc. AAS/AIAA Space Flight Mechanics Meeting*, pages 1157–1178, 2009.

[2] M L Chan, J Xie, P Fonda, H Najar, K Yamazaki, L Lin, and D A Horsley. Micromachined polycrystalline diamond hemispherical shell resonators. In *Solid-State Sensors, Actuators, and Microsystems Workshop (Hilton Head)*, pages 355–358, Hilton Head Island, South Carolina, USA, 2012.

[3] J J Bernstein, M G Bancu, E H Cook, M V Chaparala, W a Teynor, and M S Weinberg. A MEMS diamond hemispherical resonator. *Journal of Micromechanics and Microengineering*, 23(12):125007, December 2013.

[4] L. D. Sorenson, X. Gao, and F. Ayazi. 3-D micromachined hemispherical shell resonators with integrated capacitive transducers. In *IEEE MEMS*, number February, pages 168–171, January 2012.

[5] E J Eklund and A M Shkel. Self-inflated micro-glass blowing. *US Patent 8,151,600*, 2012.

[6] B Sarac, G Kumar, T Hodges, S Ding, A Desai, and J Schroers. Three-dimensional shell fabrication using blow molding of bulk metallic glass. *Journal of Microelectromechanical Systems*, 20(1):28–36, 2011.

[7] D Senkal, M J Ahamed, A A Trusov, and A M Shkel. Demonstration of sub-hz frequency symmetry in micro-glassblown wineglass resonators with integrated electrodes. In *Solid-State Sensors, Actuators and Microsystems Conference (TRANSDUCERS)*, Barcelona Spain, 2013.

[8] D Senkal, M J Ahamed, A A Trusov, and A M Shkel. High temperature micro-glassblowing process demonstrated on fused quartz and ULE TSG. *Sensors and Actuators A: Physical*, 201, December 2012.

[9] J Cho, J Yan, J A Gregory, H Eberhart, R L Peterson, and K Najafi. High-q fused silica birdbath and hemispherical 3-d resonators made by blow torch molding. In *IEEE MEMS*, pages 177–180, Taipei, Taiwan, 2013.

[10] E J Eklund and A M Shkel. Glass blowing on a wafer level. *Journal of Microelectromechanical Systems*, 16(2):232–239, April 2007.

[11] J Donea, S Giuliani, and JP Halleux. An arbitrary Lagrangian-Eulerian finite element method for transient dynamic fluid-structure interactions. *Computer Methods in Applied Mechanics and Engineering*, 33:689–723, 1982.

[12] CW Hirt, AA Amsden, and JL Cook. An arbitrary Lagrangian-Eulerian computing method for all flow speeds. *Journal of Computational Physics*, 253(14):227–253, 1974.

[13] JE Shelby. *Introduction to glass science and technology*. Royal Society of Chemistry, 2005.